Phase transition and crystal structures of $(NH_4)_2MgF_4$

1996 J. Phys.: Condens. Matter 8 8971

(http://iopscience.iop.org/0953-8984/8/46/004)

J. Phys.: Condens. Matter **8** (1996) 8971–8982. Printed in the UK

Phase transition and crystal structures of $(NH_4)_2MgF_4$

G Subías, E Palacios†, J Blasco and J García-Ruiz

Instituto de Ciencia de Materiales de Aragón, CSIC-Universidad de Zaragoza, Facultad de Ciencias, Plaza San Francisco, 50009-Zaragoza, Spain

Received 30 May 1996

Abstract. X-ray diffraction and differential scanning calorimetry experiments have made it evident that $(NH_4)_2MgF_4$ undergoes a first-order structural phase transition at 163 ± 1 K from a K_2NiF_4-type structure ($I4/mmm$) at room temperature to a monoclinic cell ($P2_1/c$) at low temperatures. The transition $I4/mmm \rightarrow P2_1/c$ arises from coupled MgF_6 tilts ϕ and θ around [110] and [001] directions of the tetragonal unit cell and have been explained in the framework of the Landau theory using an expansion of the free energy with two interacting order parameters ϕ and θ, taking into account up to sixth-order terms. The large entropy content of the transition has been explained assuming that the ammonium ion is free to rotate around the fourfold crystallographic axis in the high-temperature phase.

1. Introduction

Structural studies in compounds with the layered perovskite K_2NiF_4 structure (space group, $I4/mmm$; $Z = 2$) have regained interest in the last few years owing to the relationship with the crystallographic properties of high-T_c superconductors and related oxides RE_2MO_4 type (RE = rare earth; M = Cu, Ni or Co) [1]. This structure can be viewed as a stacking of layers of corner-sharing NiF_6 octahedra. Each layer is displaced with respect to the nearest layers by $(\boldsymbol{a}_0/2, \boldsymbol{b}_0/2, \boldsymbol{c}_0/2)$, where $\boldsymbol{a}_0, \boldsymbol{b}_0, \boldsymbol{c}_0$ are the direct cell vectors. The K ions (or rare earth ions in oxides) are located between two consecutive layers. Rotations of the octahedra produce different phases at low temperatures with lower symmetry. These phases have been classified according to the different modes of octahedra tilting [2, 3]. Some RE_2MO_4 (RE = rare earth; M = Cu, Ni or Co) oxides undergo a sequence of structural phase transitions [4, 5] from tetragonal ($I4/mmm$) to orthorhombic ($Bmab$; $Z = 4$) owing to a small rotation of the MO_6 octahedra around the $\boldsymbol{a}$ (or $\boldsymbol{b}$) axis on decreasing the temperature. The new base-centred cell has approximately the following lattice parameters: $a \approx b \approx \sqrt{2}a_0$ and $c \approx c_0$. At lower temperatures a first-order phase transition from the orthorhombic ($Bmab$) to tetragonal ($P4_2/ncm$) phase ($Z = 4$) occurs. This phase can be obtained from the $I4/mmm$ phase by a rotation of one layer of MO_6 octahedra around the $\boldsymbol{a}_0$ axis and the other layer around the $\boldsymbol{b}_0$ axis. In this structure, the new lattice parameters are also $a \approx b \approx \sqrt{2}a_0$ and $c \approx c_0$.

To our knowledge, these types of phase transition have not been described as yet for tetrafluorides. Nevertheless the ammonium fluoride perovskites are special cases. The aspherical symmetry of the NH_4^+ ion may induce other phases different from the typical cases observed in oxides. In fact, the ammonium ordering in trifluoride perovskites gives

† Author to whom correspondence should be addressed.

0953-8984/96/468971+12$19.50

rise to different crystal structures of non-ammonium isomorphous compounds. As an example, $RbMnF_3$ does not show any phase transition as a function of temperature while structural transitions in $KMnF_3$ [6] and $KCdF_3$ [7] proceed in steps from the high-symmetry phase (simple-cubic perovskite) through lower-symmetry phases down to the orthorhombic ($Pbnm$; $Z = 4$) phase. Nevertheless, the low-temperature phases ($Pbnm$) in the ammonium trifluorides NH_4MnF_3 [8] and NH_4CdF_3 [9] are reached in only one step owing to the simultaneous tilts of MF_6 (M = Mn or Cd) octahedra and ordering of the NH_4^+ ions. As we shall show in this work, the NH_4^+ ion is placed at the fourfold axis of the $(NH_4)_2MgF_4$ tetragonal structure. As the NH_4^+ ion does not have any fourfold symmetry axis, it must be disordered at least between two orientations and, therefore, an ordering process is expected at low temperatures.

$(NH_4)_2MgF_4$ has been studied in the past [10] but its structural characterization at different temperatures remains unsolved. The only available data indicate that it is isostructural to K_2NiF_4 at room temperature. Therefore, the first aim of this work is to obtain a deeper knowledge of the $(NH_4)_2MgF_4$ structure and the possible phase transitions produced by decreasing the temperature. Moreover, $(NH_4)_2MgF_4$ is a good candidate for a structural study, since the high hydrogen content makes it inadequate for a neutron diffraction experiment, but the relatively low atomic numbers of N, F and Mg give good possibilities of localizing the H atoms by a powder x-ray diffraction experiment.

2. Experimental details

The polycrystalline sample was prepared by heating a mixture of $MgCO_3$ and NH_4F at 473 K, for 3 d [10] in a Teflon sample holder. The excess of NH_4F was removed by annealing at 420 K in a gentle Ar flow. Differential scanning calorimetry (DSC) measurements were performed between 100 K and room temperature (RT) in a Perkin–Elmer DSC7 instrument. Data on the energy power versus T were converted to molar heat capacity C_p by calibration with α-Al_2O_3.

X-ray diffraction was carried out with a D-max Rigaku diffractometer using a rotating-anode generator as source. The generator was operated at 45 kV and 160 mA, and Cu K_α (1.5418 Å) radiation was selected using a graphite monochromator. A continuous-helium-flow cryostat from Oxford Instruments was coupled to the goniometer for the measurements at low temperatures. Temperature control was better than 0.1 K and the precision in absolute temperature was checked at 107 K measuring the splitting of the diffraction peaks (200) and (002) of NH_4MgF_3, which has a first-order structural transition from cubic to tetragonal at 107.5 ± 0.1 K [11]. This splitting was clearly detected at 107 K and undetected at 108 K. Step-scanned diffractograms, using an aluminium plate as sample holder, were taken at 20 K from $2\theta = 5^\circ$ to $2\theta = 120^\circ$ in steps of 0.024° and a counting rate of 5 s/step. A glass plate was used for RT measurements without the cryogenic system. The pattern was collected between 10° and 80° every 0.024° with a counting rate of 8 s/step. Refinement of the powder patterns was performed using the FULLPROF computer program [12].

3. Results

3.1. Room-temperature phase

The high-resolution x-ray powder diffractogram of $(NH_4)_2MgF_4$ at RT is shown in figure 1. The diffractogram is consistent with a K_2NiF_4-type structure ($I4/mmm$,), as previously reported [10]. Neither the z coordinates of F and NH_4^+ nor the hydrogen atomic positions

were reported. About 4 wt% NH_4MgF_3 was also detected. We have performed a Rietveld refinement using a pseudo-Voigt profile function as peak diffraction shape without including the hydrogen atoms; the Rietveld profile reliability was $R_{wp} = 13.4\%$ and the Bragg factor $R_B = 10.4\%$ [12]. Since the peaks are well separated, the integrated intensities were used for the localization of the H atoms. The Fourier difference method gave only one physically reasonable clear peak at the position (1/2, 1/2, 0.77), located 0.99 Å from the N atom along the shortest N–F path. Consequently, the NH_4^+ ion has one N–H bond along the fourfold axis of the tetragonal ($I4/mmm$) structure and the other three form a regular triangle perpendicular to it. The orientation of the molecule can be fully specified given the rotation angle ω around the fourfold axis.

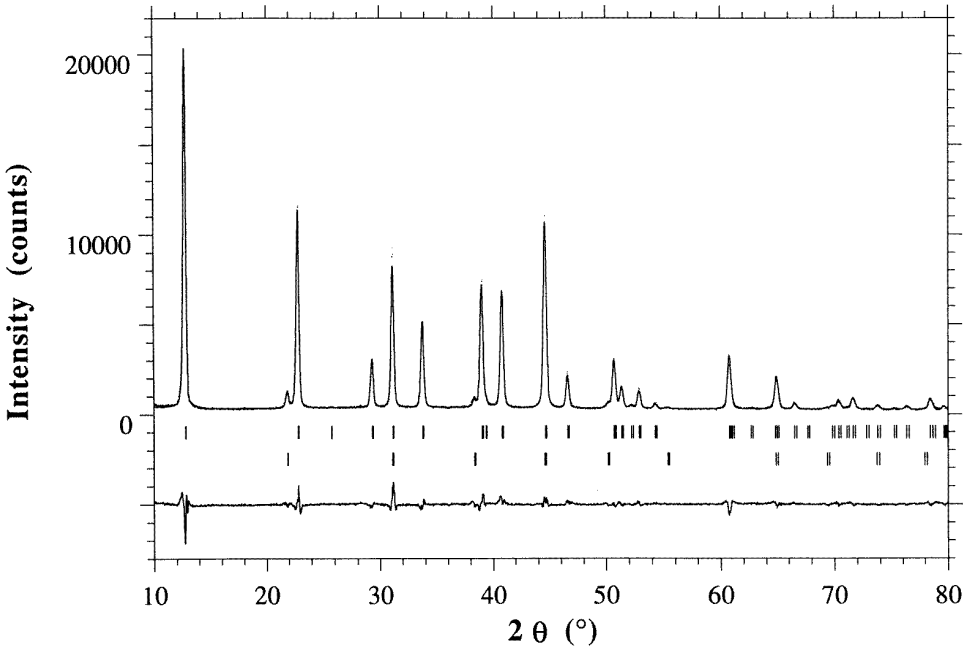

Figure 1. X-ray powder diffraction pattern (•) and best fit (——) of $(NH_4)_2MgF_4$ at RT. The bars denote the calculated Bragg reflections for $(NH_4)_2MgF_4$ (first line) and for the small impurity NH_4MgF_3 (second line). The difference between the calculated and experimental diffractogram is plotted at the bottom.

In order to investigate the orientation of the ammonium ion, the potential energy as a function of the angle ω has been calculated. The electrostatic potential energy has been computed considering only the nearest neighbours of the ammonium and assuming all ions as point charges [13], i.e. F with -1e, Mg with $+2$e and an overall charge on NH_4^+ of $+1$e. No interaction between ammonium ions has been considered. The point charges reported for H in ammonium group ranges from $+0.18$e to $+0.5$e [14]. We have taken a value of $+0.42$e in this work for each H [13, 15], this was checked satisfactorily in previous neutron diffraction work on a related compound [8]. Let the reference point be $\omega = 0$, when a H atom is in the direction of the $\boldsymbol{a}_0$ axis of the tetragonal structure; taking into account that the NH_4^+ molecule has a threefold symmetry axis coincident with the fourfold symmetry

axis of the tetragonal unit cell, the rotational potential can be written as

$$V(\omega) = V_0 + V_1\cos(12\omega) + V_2\cos(24\omega) + \cdots \tag{1}$$

which in a first-order approximation gives the equilibrium orientations $\omega_{eq} = 0\ (+2\pi n/12)$ for $V_1 < 0$, or $\omega_{eq} = \pi/12(+2\pi n/12)$ for $V_1 > 0$. The resulting V_1 is of the order of a few kelvins; so $V(\omega)$ is quasi-independent of ω. This result implies that a preferred orientation of the ammonium ion does not exist and it is free to rotate around the fourfold axis at room temperature.

The final fitting parameters are shown in table 1 and the relevant interatomic distances are given in table 2. The best fit has been obtained by locating one H atom along the fourfold axis, i.e. the 4e Wyckoff position. The other three H atoms are placed at the 32o(2H) and 16m(1H) positions with a 1/4 occupancy ($\omega_{eq} = \pi/12$). A fit with $\omega_{eq} = 0$ did not give a better R_B. The large thermal parameters obtained for these H are consistent with a free rotation of these H atoms around the fourfold axis. In this structure, owing to virtual absence of overlapping in the diffraction peaks, the most relevant reliability index is R_B calculated for the integrated intensities of the peaks. Some other possibilities of the tetrahedral orientation (i.e. without one N–H bond along the $\boldsymbol{c}$ axis) have also been tested, but they gave much poorer fits to the experimental diffractogram and energies of thousands of kelvins higher than described above.

Table 1. Refined fractional atomic positions, thermal parameters B and unit-cell parameters ($(NH_4)_2MgF_4$, 300 K; space group, $I4/mmm$; $Z = 2$; $a = 4.0567(1)$ Å; $c = 13.8354(6)$ Å; Bragg reliability factor $R_B = 3.4\%$; Rietveld unweighted factor $R_P = 7.4\%$; Rietveld weighted factor $R_{wp} = 9.4\%$). The standard errors in parentheses refers to the least significant digit. The coordinates of hydrogen atoms are constrained to form a regular tetrahedron centred in the N atom. Each kind of atom has an unique isotropical thermal parameter.

Atom	Position	x	y	z	B (Å^2)	Occupancy
N	4e	1/2	1/2	0.8412(2)	3.7(1)	1
H(1)	4e	1/2	1/2	0.7675	9.1(9)	1
H(2)	32o	0.7289	0.5613	0.8659	9.1(9)	0.25
H(3)	16m	0.3324	0.6675	0.8659	9.1(9)	0.25
Mg	2a	0	0	0	3.9(1)	1
F(1)	4e	0	0	0.1444(2)	4.0(1)	1
F(2)	4c	1/2	0	0	4.0(1)	1

3.2. Low-temperature phase

The x-ray powder pattern of $(NH_4)_2MgF_4$ at 20 K is shown in figure 2. New diffraction peaks appear and some peaks of the high-temperature phase are split in the low-temperature diagram. All attempts to index the pattern following the computational methods of trial and error were unsuccessful in giving physically acceptable solutions. Therefore, a different procedure was used, taking information not only from the position of the lines but also from their intensity. It is expected that the low-temperature structure will arise from the RT phase by small tilts of the MgF_6 octahedra, which would produce splittings of the RT diffraction lines (substructure lines) due to the distortion of the tetragonal cell, with only slight changes in the intensities of the single lines. The new weak reflections (superstructure lines) would indicate a larger unit cell than at RT. The first step was to find the distortion of the subcell. Dividing the integrated intensities of the RT phase by their multiplicity, we

Table 2. Characteristic interatomic distances and angles at 300 K with their standard deviations.

MgF_6 octahedra		N environment	
Atoms	Distance (Å)	Atoms	Distance (Å)
Mg–F(1)	1.997(3)	N–F(1)(i)[b]	2.724(4)
Mg–F(1)(i)[a]	1.997(3)	N–F(1)(ii)[b]	2.875(1)
Mg–F(2)	2.028(1)	N–F(1)(iii)[b]	2.875(1)
Mg–F(2)(ii)[a]	2.028(1)	N–F(1)(iv)[b]	2.875(1)
Mg–F(2)(iii)[a]	2.028(1)	N–F(1)(v)[b]	2.875(1)
Mg–F(2)(iv)[a]	2.028(1)	N–F(2)(vi)[b]	2.989(2)
⟨Mg–F⟩	2.018	N–F(2)(vii)[b]	2.989(2)
		N–F(2)(viii)[b]	2.989(2)
		N–F(2)(ix)[b]	2.989(2)

[a] Symmetry codes: (i) $x, y, -z$; (ii) $x-1, y, z$; (iii) $-y, x, z$; (iv) $-y, x-1, z$.
[b] Symmetry codes: (i) $x+0.5, y+0.5, z+0.5$; (ii) $x, y, 1-z$; (iii) $x, y+1, 1-z$; (iv) $x+1, y, 1-z$; (v) $x+1, y+1, 1-z$; (vi) $x, y, z+1$; (vii) $x, y+1, z+1$; (viii) $-y, x, z+1$; (ix) $1-y, x, z+1$.

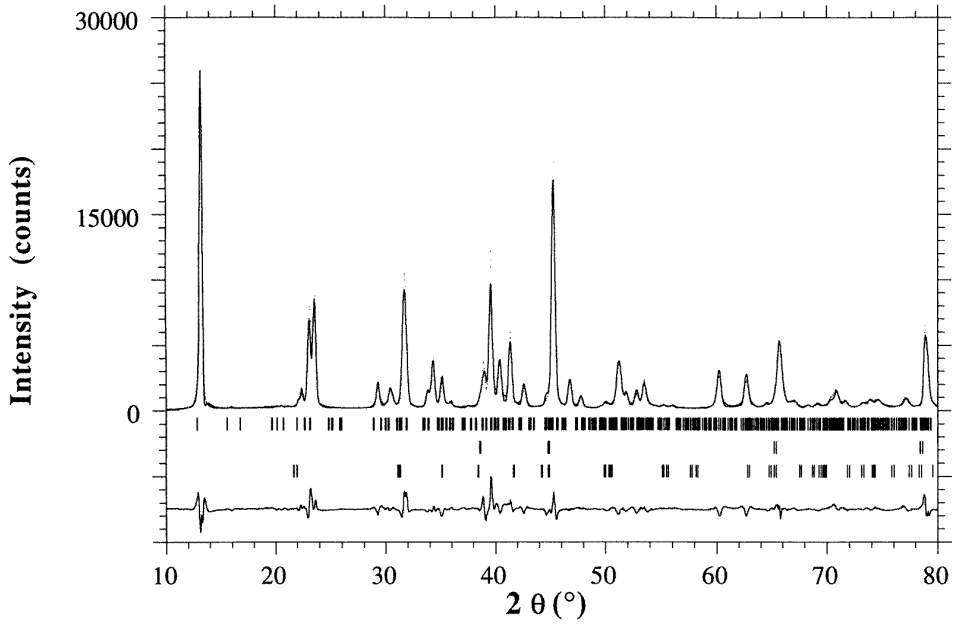

Figure 2. X-ray diffraction pattern at 20 K of $(NH_4)_2MgF_4$ (•) and calculated profile (——). The bars denote the calculated Bragg reflections for $(NH_4)_2MgF_4$ (first row), small impurities from the aluminium sample holder (second row) and NH_4MgF_3 (third row). The difference between experimental and calculated patterns is shown at the bottom.

get a collection of indexed substructure reflections with approximate values of intensity. A calculated diffraction pattern may be made assuming the same width as at RT for the reflections, for any choice of a, b, c, α, β and γ subcell parameters. The possible structures given by Aleksandrov *et al* [2] were taken as a guide in order of descending symmetry from the $I4/mmm$ structure. Going on with this procedure it is clear that no orthorhombic structure can explain the observed splitting of the (101) line of the $I4/mmm$ structure, which

would give (111) and $(1\bar{1}1)$. A more careful analysis, by fitting a, b, c and β, showed the structure number 16 in table 1 of Aleksandrov *et al* [2] as the only physically acceptable possibility. This result implies the following tilts of the MgF_6 octahedra: an alternate rotation around the $\boldsymbol{c}_0$ axis $+\theta$ and $-\theta$ in alternate layers, and simultaneous rotations of the alternate layers by an angle ϕ, around the $\boldsymbol{a}_0$ or $\boldsymbol{b}_0$ axes, respectively. That gives a new cell with approximate lattice parameters $a \approx b \approx \sqrt{2}a_0$ and $c \approx c_0$ and a new monoclinic space group $P2_1/c$, with $Z = 4$.

The angles ϕ and θ were the only atomic positional fitting parameters in the first trials of the refinement by the Rietveld method. In the next steps all non-hydrogen atomic positions and thermal parameters as well as the unit-cell and instrumental parameters were refined, giving a final $R_B = 15.3\%$. Finally the position of hydrogen atoms were deduced assuming the NH_4^+ to be a rigid regular tetrahedron, and refining the three angles which define the orientation of each molecule with respect to the crystal lattice. The orientation found is physically reasonable and coincides with the minimum electrostatic energy, calculated as for the high-temperature phase. The small thermal parameters for the H atoms indicate that ammonium ion is in a fixed configuration in the low-temperature phase. The final fitting parameters are listed in table 3 and the relevant interatomic distances are given in table 4. It is of interest to examine only the intensity data for $10^\circ < 2\theta < 80^\circ$, because the scattering amplitude becomes very weak for light atoms at large diffraction angles (above $2\theta = 80^\circ$ the most relevant peaks are produced by the Al sample holder).

Table 3. Refined fractional atomic positions, thermal parameters B and unit-cell parameters ($(NH_4)_2MgF_4$, 20 K; space group, $P2_1/c$; $Z = 4$; $a = 5.7039(7)$ Å; $b = 5.7298(8)$ Å; $c = 13.821(2)$ Å; $\beta = 86.995(7)^\circ$; Bragg reliability factor $R_B = 5.58\%$; Rietveld unweighted factor $R_P = 10.4\%$; Rietveld weighted factor $R_{wp} = 13.6\%$). The standard error in parentheses refers to the least significant digit. H atoms are constrained to form regular tetrahedra centred in N. The standard deviation of orientation is 5°. All atoms of the same kind have a unique thermal parameter.

Atom	Position	x	y	z	B (Å^2)
N(1)	4e	0.4962(39)	0.0144(84)	0.1561(12)	0.5(3)
N(2)	4e	−0.0289(37)	0.4836(81)	0.1598(11)	0.5(3)
Mg(1)	2a	0	0	0	1.2(1)
Mg(2)	2d	1/2	1/2	0	1.2(1)
F(1)	4e	−0.0053(30)	0.0173(62)	0.1487(9)	0.9(1)
F(2)	4e	0.4913(31)	0.4806(61)	0.1381(9)	0.9(1)
F(3)	4e	0.7795(17)	0.2580(28)	−0.0029(9)	0.9(1)
F(4)	4e	0.2523(18)	0.2270(24)	−0.0116(9)	0.9(1)
H(1)	4e	0.3422	−0.0681	0.1314	0.5(3)
H(2)	4e	0.4987	0.1850	0.1314	0.5(3)
H(3)	4e	0.4814	0.0140	0.2301	0.5(3)
H(4)	4e	0.6645	−0.0764	0.1314	0.5(3)
H(5)	4e	−0.0381	0.5057	0.2333	0.5(3)
H(6)	4e	−0.1846	0.5401	0.1332	0.5(3)
H(7)	4e	−0.0032	0.3085	0.1435	0.5(3)
H(8)	4e	0.1090	0.5802	0.1292	0.5(3)

The final angles were $|\theta| \approx 3^\circ$ and $\phi \approx 4^\circ$. The motion of the octahedra induces the approach of four fluorine atoms to the ammonium ion (see table 4) in such a way that the NH_4^+ ions (freely rotating around the $\boldsymbol{c}$ axis at RT) choose the orientation of the minimum distances between the nearest fluorine atoms and the hydrogen atoms.

Table 4. Characteristic interatomic distances and angles at 20 K with their standard deviations.

MgF_6 octahedra						N environment			
Atoms	Distance (Å)	Angle (deg)	Atoms	Distance (Å)	Angle (deg)	Atoms	Distance (Å)	Atoms	Distance (Å)
Mg(1)–F(1)	2.056(12)		Mg(2)–F(2)	1.910(12)		N(1)–F(1)	2.867(28)[b]	N(2)–F(1)	2.680(58)[b]
Mg(1)–F(1)(i)[a]	2.056(12)		Mg(2)–F(2)(iv)[a]	1.910(12)		N(1)–F(1)(i)[c]	2.839(28)	N(2)–F(1)(v)[c]	3.064(58)
Mg(1)–F(3)(ii)[a]	1.943(14)		Mg(2)–F(3)	2.112(13)		N(1)–F(2)(ii)[c]	3.069(59)	N(2)–F(1)(vi)[c]	2.671(20)[b]
Mg(1)–F(3)(iii)[a]	1.943(14)		Mg(2)–F(3)(iv)[a]	2.112(13)		N(1)–F(2)	2.683(59)[b]	N(2)–F(2)(vii)[c]	2.768(28)[b]
Mg(1)–F(4)	1.940(12)		Mg(2)–F(4)	2.119(12)		N(1)–F(2)(iii)[c]	2.856(21)[b]	N(2)–F(2)	2.967(28)
Mg(1)–F(4)(i)[a]	1.940(12)		Mg(2)–F(4)(iv)[a]	2.119(12)		N(1)–F(3)	3.003(31)	N(2)–F(3)(vii)[c]	2.860(29)
⟨Mg(1)–F⟩	1.979		⟨Mg(2)–F⟩	2.047		N(1)–F(3)(iv)[c]	3.121(32)	N(2)–F(3)(viii)[c]	2.931(31)[b]
⟨F(i)–Mg(1)–F(j)⟩		88–92	⟨F(i)–Mg(2)–F(j)⟩		87–93	N(1)–F(4)	3.021(28)	N(2)–F(4)	3.154(29)
						N(1)–F(4)(iv)[c]	2.767(31)[b]	N(2)–F(4)(ix)[c]	2.973(32)

[a] Symmetry codes: (i) $-x, -y, -z$; (ii) $x-1, y, z$; (iii) $1-x, -y, -z$; (iv) $1-x, 1-y, -z$.
[b] Fluorine atoms which form a nearly tetrahedral cage for NH_4^+ ion.
[c] Symmetry codes: (i) $x+1, y, z$; (ii) $x, y-1, z$; (iii) $1-x, y-0.5, 0.5-z$; (iv) $1-x, -y, -z$; (v) $x, y+1, z$; (vi) $-x, y+0.5, 0.5-z$; (vii) $x-1, y, z$; (viii) $1-x, 1-y, -z$; (ix) $-x, 1-y, -z$.

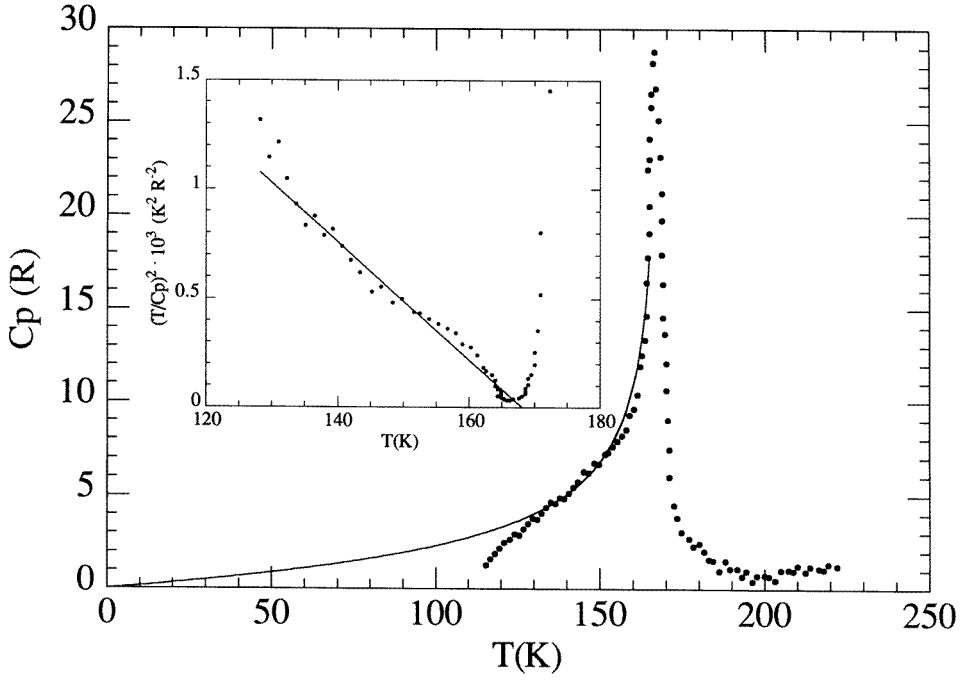

Figure 3. Anomalous heat capacity of $(NH_4)_2MgF_4$ obtained from linear extrapolation from the high-temperature data to low temperatures: ——, the Landau prediction. The linearity of $(T/\Delta C_p)^2$ versus temperature is shown in the inset: ——, guide for the eyes.

3.3. Differential scanning calorimetry

DSC experiments between 100 and 300 K have shown a sharp anomaly at around 165 K. The hysteresis of the detected phase transition has been determined by means of heating and cooling scans at different scanning rates. We have obtained from the extrapolation to zero velocity the temperature of the phase transition and the thermal hysteresis ($\Delta T = 1.8$ K) from the difference between the temperatures from the extrapolated heating and cooling processes. The anomalous contribution ΔC_p, shown in figure 3, has been estimated by subtraction of a linear extrapolation of the C_p values down to $T < T_0$, after subtracting the rotational contribution (approximately $\Delta C_p = R$) at high temperatures, in order to take into account the free rotation of NH_4^+ ions. $(T/\Delta C_p)^2$ for $T < T_0$ is linear close to T_0, in good agreement with the Landau prediction for the first-order transition as is shown in the inset of figure 1. The anomalous entropy ΔS and enthalpy ΔH have been obtained by integration of the Landau curve below 132 K and the experimental data above this temperature owing to the uncertain estimation for C_p far below the transition. The resulting values are $\Delta S/R = 5.2 \pm 0.8$ and $\Delta H/R = 593 \pm 86$ K ($R = 8.3143$ J mol^{-1} K^{-1}); the large errors come from the difficult estimation of the anomalous contribution at low temperatures.

4. Discussion

As we have shown, $(NH_4)_2MgF_4$ undergoes a first-order structural phase transition at 163 K from $I4/mmm$ to $P2_1/c$ symmetry. This phase transition is produced by the simultaneous

rotation of the MgF_6 octaedra by θ and ϕ. A pictorial view of the low-temperature phase unit cell, where the octahedra tilts are overemphasized, is shown in figure 4 together with the high-temperature unit cell indicated by broken lines. In the high-temperature phase the electrostatic potential owing to the neighbouring atoms of the ammonium ion allows the free rotation of this ion around the tetragonal fourfold axis. The structural changes in the low-temperature phase, on the contrary, induce an approach of four of the fluorine atoms to the ammonium ion and its position is fixed. Consequently, the structural change is accompanied by an ordering of the orientation of NH_4^+. The large anomaly found in the calorimetric measurements can be explained as owing to the gain of entropy (enthalpy) coming from the transition of the NH_4^+ ion from a fixed state to free rotation. In fact, the anomalous entropy calculated up to 180 K gives a value of $\Delta S/R = 5.2$, which agrees with twice the molar entropy of a rotor with a fixed axis (note that there are two NH_4^+ ions per unit formula), $\Delta S/R = 2.60$ (180 K). The molar entropy of a rotor with a fixed axis is given by $\Delta S/R = \frac{1}{2} + \ln\sqrt{2\pi I k_B T/\hbar^2}$ in the high-temperature limit, I being the moment of inertia of the NH_4^+ ion. Therefore, the calorimetric data are close to the one-dimensional free-rotor case, in good agreement with the crystallographic results.

The phase transition in $(NH_4)_2MgF_4$ originated from the instability of the octahedral units with respect to definite types of rotational distortion (θ and ϕ tilts). These tilts of the octahedra are similar to those observed in the lowest-temperature phase of the $(CH_3NH_3)_2CdCl_4$ [16] and $(CH_3NH_3)_2MnCl_4$ [17] dielectrics, but in these last cases the symmetry reduction occurs in three steps: $I4/mmm$ (T1) $\rightarrow$ $Bmab$ (O1) $\rightarrow$ $P4_2/ncm$ (T2) $\rightarrow$ $P2_1/c$(M). The first two transitions are very common also in RE_2MO_4 [4, 5]. In the notation of [2], the orthorhombic (O1) and low-temperature tetragonal phases (T2) correspond to the same irreducible representation (IR) τ_3 of the X point in the Brillouin zone of the high-temperature tetragonal (T1) phase. Then, this T1–O1–T2 sequence is explained including sixth-order terms in the Landau expansion of the free energy [5]:

$$F = F_0 + \frac{a}{2}(T - T_{c2})(\phi_1^2 + \phi_2^2) + \frac{v}{4}(\phi_1^4 + \phi_2^4) + \gamma\phi_1^2\phi_2^2 + \frac{u}{6}(\phi_1^2 + \phi_2^2)^2(\phi_1^2 - \phi_2^2) + \frac{c}{2}\eta^2 + \zeta\eta(\phi_1^2 - \phi_2^2)$$

where ϕ_1 and ϕ_2 are the two components of the IR τ_3 order parameter and η is related to the orthorhombic strain. Physically, ϕ_1 and ϕ_2 represent the rotation angles of the octahedra along [110] (ϕ_1) and [1$\bar{1}$0] (ϕ_2) directions of the $I4/mmm$ phase. In the T1 phase, $\phi_1 = \phi_2 = \eta = 0, v < 0$. In the O1 phase, $\eta \neq 0$ and either $\phi_1 \neq 0$ and $\phi_2 = 0$, or $\phi_2 \neq 0$ and $\phi_1 = 0$. In the T2 phase, $\eta = 0$, $|\phi_1| = |\phi_2| \neq 0$ and $v > 0$. Therefore, the O1 $\rightarrow$ T2 transition is associated with the change in the sign of v at the transition temperature.

To interpret the monoclinic phase $P2_1/c$, another two-component order parameter which corresponds to the IR τ_7 is needed. The transitions associated with this IR τ_7 of the same X point in the Brillouin zone would give two new phases. In this case, the two components θ_1 and θ_2 of the order parameter represent the rotation angles of the two layers around the $\boldsymbol{c}$ axis (i.e. θ_1 tilt of layer 1 and θ_2 tilt of layer 2). This IR alone could produce first a tetragonal (T3) phase $P4/mbm$; ($Z = 4$) with $\theta_1 \neq 0$ and $\theta_2 = 0$, or $\theta_1 = 0$ and $\theta_2 \neq 0$ and secondly an orthorhombic (O2) phase ($Bbcm$) with $|\theta_1| = |\theta_2| \neq 0$.

The monoclinic phase M, found in this work, is obtained when $|\phi_1| = |\phi_2| \neq 0$ and $\theta_1 = -\theta_2 \neq 0$. Then, the Landau free energy should include terms depending on the four parameters ϕ_1, ϕ_2, θ_1 and θ_2. We have assumed for simplicity that $\phi = |\phi_1| = |\phi_2|$ and $\theta = \theta_1 = -\theta_2$. A Landau expansion keeping terms up to fourth order only cannot explain a direct transition from the T1 phase to the M phase, except from the second-order point.

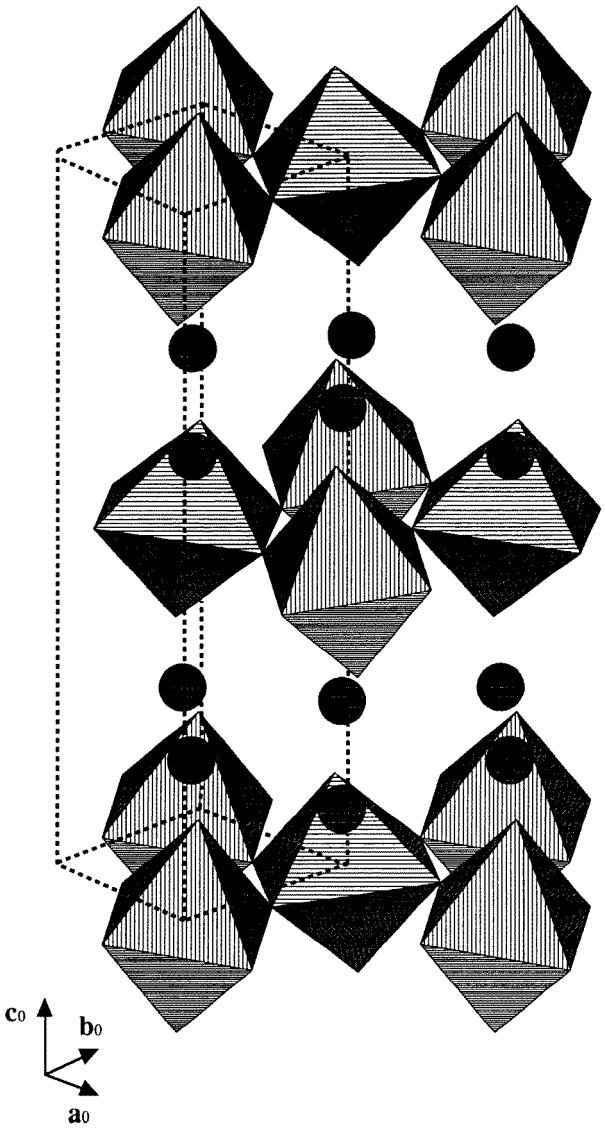

Figure 4. Crystallographic unit cell of $(NH_4)_2MgF_4$ at low temperatures ($P2_1/c$ symmetry). Broken octahedra correspond to the MgF_6 units and circles to the amonium ions. The high-temperature unit cell is also displayed as broken lines.

Consequently, the simplest expansion of the free energy to reproduce the present transition is written as [18]

$$F = F_0 + \frac{\alpha_1}{2}\phi^2 + \frac{\beta_1}{4}\phi^4 + \frac{\gamma_1}{6}\phi^6 + \frac{\alpha_2}{2}\theta^2 + \frac{\beta_2}{4}\theta^4 + \frac{\gamma_2}{6}\theta^6 + \frac{\delta}{2}\phi^2\theta^2$$

with $\alpha_1 = a_1(T - T_{c1})$, $\alpha_2 = a_2(T - T_{c2})$, $\gamma_1 > 0$ and $\gamma_2 > 0$. Large negative values of δ ($\delta < -\sqrt{|\beta_1||\beta_2|}$) as well as either both $\beta_1, \beta_2 < 0$, or at least one of them negative, are necessary to describe a first-order transition between the T1 and M phases. Depending on

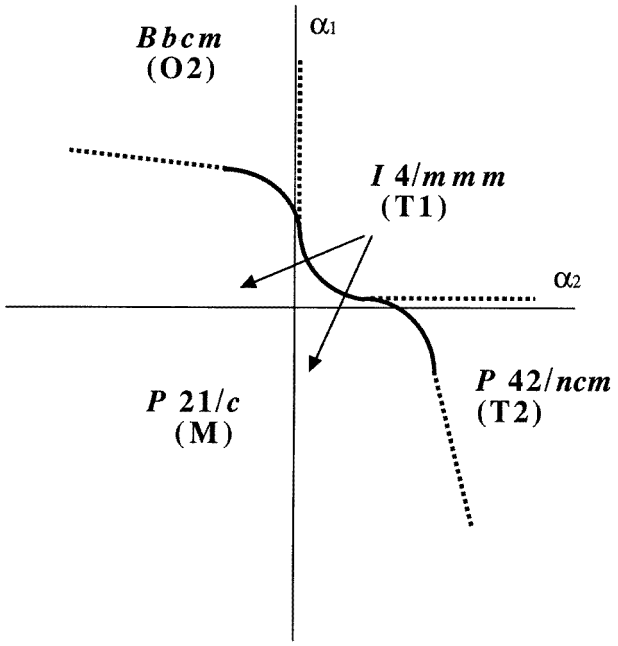

Figure 5. Phase diagrams in the (α_1, α_2) plane for γ_1 and $\gamma_2 > 0, \beta_1 > 0, \beta_2 < 0, \Delta < 0$ and $\delta < 0$: ——, first-order phase transitions; – – –, second-order phase transitions.

the sign of β_1 and β_2, three different cases are possible. We have reproduced in figure 5 the phase diagram in the (α_1, α_2) plane corresponding to $\beta_1 > 0$ and $\beta_2 < 0$. The conclusions derived from our discussion are also valid for the other two cases and they are not reproduced here [19]. Assuming constant values for $\beta_1, \beta_2, \gamma_1, \gamma_2$ and δ at different temperatures, the state points lie on the straight line

$$\alpha_1 = \frac{a_1}{a_2}\alpha_2 + a_1(T_{c2} - T_{c1})$$

ending at the point defined by $\alpha_1 = -a_1 T_{c1}$ and $\alpha_2 = -a_2 T_{c2}$, which allows a first-order transition at $T_0 = 163$ K, directly from the T1 to the M phase if T_{c2} is close to T_{c1}. Otherwise there are two transitions, namely one from T1 to T2 and the other from T2 to M, as has been observed in tetrachlorides [16, 17]. Besides, if T_{c1} is high enough and $T_{c2} < 0$ the M phase is not reached at any temperature; consequently, there is only a transition from T1 to T2 or O1 as occurs in RE_2MO_4 where $|\phi_1| \neq |\phi_2|$ is allowed.

Several phenomenological theories have been proposed to explain the observed phase sequences in oxides and tetrachlorides with general formula A_2BX_4 [4, 16, 20]. However, it is the first time that a direct first-order transition, as reported in this paper, is found experimentally in this family of crystals. We have proposed a Landau-type free-energy function which interprets all these phase sequences, including this direct transition from the T1 to the M phase. In particular, the high-symmetry phase of $(NH_4)_2MgF_4$ is unstable in the presence of two types of distortion (θ and ϕ tilts) of different symmetries which interact non-linearly. This interaction term is necessary to explain the main characteristics of the transition, as its first-order character together with the simultaneous ordering of ammonium ions and tilts of octahedra. As in cubic compounds, NH_4MF_3 (M = Cu, Ni, etc), where the condensation of the two modes R_{25} and M_3 govern the minimum-energy order of ammonium

ions [8], the transition in $(NH_4)_2MgF_4$ is described by coupling the tilts of the octahedra by means of the reorientation of ammonium ions.

5. Conclusions

$(NH_4)_2MgF_4$ has a tetragonal unit cell at RT well explained using the $I4/mmm$ spatial group. Both x-ray diffraction measurements and DSC measurements indicate that NH_4^+ is a freely rotating molecule around its threefold axis which lies in the fourfold crystalline axis.

This compound shows a structural transition owing to the tilts of the MgF_6 octaedra. The structure at low temperatures shows a monoclinic unit cell, well described by the spatial group $P2_1/c$. The NH_4^+ ions are fixed in this unit cell, leading to minimum distances between the H and F atoms that is the minimum-energy structure.

This kind of direct transition is very unusual in related compounds such as oxides and tetrachlorides but can be perfectly explained in the framework of the Landau theory with two non-linear interacting order parameters using an expression for the expansion of the free energy up to sixth-order terms in both order parameters.

Acknowledgment

This work was made possible by the generous financial support of the Comisión Interministerial de Ciencia y Tecnología (project PB92-1077).

References

[1] See for example Goodenough J B and Manthiram A 1990 *J. Solid State Chem.* **88** 115
Rice D E and Buttrey D J 1993 *J. Solid State Chem.* **105** 197
[2] Aleksandrov K S, Beznosikov B V and Misyul S V 1987 *Phys. Status Solidi* a **104** 529
[3] Aleksandrov K S and Bartolomé J 1994 *J. Phys.: Condens. Matter* **6** 8219
[4] Ishibashi Y and Dvroak V 1994 *J. Phys. Soc. Japan* **63** 2202
[5] Martínez J L, Fernández-Díaz MT and Rodríguez-Carvajal J 1991 *Phys. Rev.* B **43** 13 766
[6] Hidaka M, Fuji H and Maeda S 1986 *Phase Trans.* **6** 114
[7] Darlington C N W 1984 *J. Phys. C: Solid State Phys.* **17** 2859
[8] Rubín J, Palacios E, Bartolomé J and Rodríguez-Carvajal J 1995 *J. Phys.: Condens. Matter* **7** 563
[9] Le Bail A, Fourquet J L, Rubín J, Palacios E and Bartolomé J 1990 *Physica* B **162** 231
[10] Charpin P, Roux N and Ehretsmann J 1968 *C. R. Acad. Sci. Paris* C **267** 484
[11] Palacios E, Navarro R, Burriel R, Bartolomé J and González D 1986 *J. Chem. Thermodyn.* **18** 1089
[12] Rodríguez-Carvajal J L, Anne M and Pannetier J 1987 *ILL Report* 87**R**014**T**
[13] Plumb R C and Hornig D F 1995 *J. Chem. Phys.* **23** 947
[14] Goodliff A L, Jenkins H D B, Martin S V 1971 *Mol. Phys.* **21** 761
[15] Bartolomé J, Navarro R, Gonzalez D and Jongh L J 1977 *Physica* B **92** 23
[16] Chapuis G, Kind R and Arend H 1976 *Phys. Status Solidi* a **36** 285
[17] Knorr K, Jahn I R and Heger G 1974 *Solid State Commun.* **15** 231
[18] Tolédano J C and Tolédano P 1987 *The Landau Theory of Phase Transitions (World Scientific Lect. Notes Phys. 3)* (Singapore: World Scientific) ch IV
[19] Gufan Y M and Larin E S 1980 *Sov. Phys. – Solid State* **22** 270
[20] Axe J D, Moudden A H, Holwein D, Cox D E, Mohanty K M, Moodenbaugh A R and Youwen X 1989 *Phys. Rev. Lett.* **62** 2751